ACS EARTH AND SPACE CHEMISTRY

http://pubs.acs.org/journal/aesccq

Article

Polycyclic Aromatic Hydrocarbons (PAHs) in Interstellar Ices: A Computational Study into How the Ice Matrix Influences the Ionic State of PAH Photoproducts

Stephanie ten Brinck, Celine Nieuwland, Angela van der Werf, Richard M. P. Veenboer, Harold Linnartz, F. Matthias Bickelhaupt,* and Célia Fonseca Guerra*

Cite This: *ACS Earth Space Chem.* 2022, 6, 766−774

Read Online

ACCESS | Metrics & More | Article Recommendations | Supporting Information

ABSTRACT: It has been experimentally observed that water−ice-embedded polycyclic aromatic hydrocarbons (PAHs) form radical cations when exposed to vacuum UV irradiation, whereas ammonia-embedded PAHs lead to the formation of radical anions. In this study, we explain this phenomenon by investigating the fundamental electronic differences between water and ammonia, the implications of these differences on the PAH−water and PAH−ammonia interaction, and the possible ionization pathways in these complexes using density functional theory (DFT) computations. In the framework of the Kohn−Sham molecular orbital (MO) theory, we show that the ionic state of the PAH photoproducts results from the degree of occupied−occupied MO mixing between the PAHs and the matrix molecules. When interacting with the PAH, the lone pair-type highest occupied molecular orbital (HOMO) of water has poor orbital overlap and is too low in energy to mix with the filled π-orbitals of the PAH. As the lone-pair HOMO of ammonia is significantly higher in energy and has better overlap with filled π-orbitals of the PAH, the subsequent Pauli repulsion leads to mixed MOs with both PAH and ammonia character. By time-dependent DFT calculations, we demonstrate that the formation of mixed PAH−ammonia MOs opens alternative charge-transfer excitation pathways as now electronic density from ammonia can be transferred to unoccupied PAH levels, yielding anionic PAHs. As this pathway is much less available for water-embedded PAHs, charge transfer mainly occurs from localized PAH MOs to mixed PAH−water virtual levels, leading to cationic PAHs.

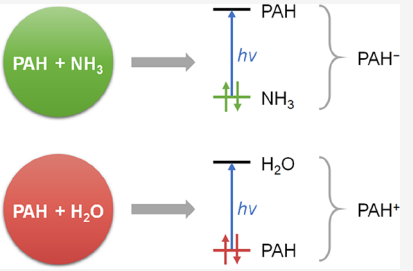

KEYWORDS: *astrochemistry, density functional theory, charge-transfer excitations, ice-matrix effects, photoproducts, polycyclic aromatic hydrocarbons (PAHs)*

1. INTRODUCTION

The presence of polycyclic aromatic hydrocarbons (PAHs) in the interstellar medium has been proven through the presence of strong infrared (IR) emission bands between 3.3 and 11.3 μm.[1] For quite some time, these IR emission features could not be explained and therefore were named the unidentified IR features. In the 80s, these features were hypothesized to originate from various stretching and bending modes of vibrationally excited hydrocarbon systems, such as PAHs, after excitation by photons from the interstellar radiation field.[1b−d,g,2] Nowadays, the existence of interstellar PAHs is generally accepted, specifically after the recent unambiguous astronomical identification of a number of aromatic species.[3] Organic molecules such as PAHs play an important role in interstellar chemistry. They are formed in the outflows of dying stars, contribute upon fragmentation to the molecular inventory in space, and are expected to freeze out onto cold dust grains. Here, they get embedded in an ice matrix comprising mainly water but that also comprises other species that are expected to form upon the solid-state hydrogenation of atomic precursors, such as ammonia.[4,5] Although water−ice is the main component of interstellar ice analogues, observations with the Spitzer Space Telescope showed that ammonia can be present in water-rich ices, with an abundance typically 10−20 times lower with respect to water.[6] Upon exposure to high-energy irradiation, reactions of PAHs or PAH derivatives with the surrounding matrix are expected to occur. In fact, the vacuum UV (VUV) irradiation and particle bombardment of these interstellar ices produces complex organic molecules that possibly played a vital role in the origin of life.[7]

Previous *in situ* spectroscopic studies have shown that PAHs embedded in a water−ice matrix are readily ionized.[8,9] For example, Gudipati and Allamandola showed that 4-methylpyrene, naphthalene, and quaterrylene in water−ice can be ionized

Received: December 13, 2021
Revised: January 24, 2022
Accepted: February 8, 2022
Published: February 21, 2022

by Lyman-α (10.2 eV) irradiation to their cationic forms.[8] Similarly, Kofman *et al.* and Bouwman *et al.* observed the formation of cationic triphenylene and pyrene, respectively, in water−ice at 20 K when exposed to VUV broadband irradiation (120−160 nm) by recording the time-resolved electronic spectra of these PAHs as a function of fluence.[9,10] In the study of Bouwman *et al.*, the authors state that the photolysis of pyrene is the result of direct single-photon ionization of the neutral species. In 2012, however, Cuylle *et al.* showed that both pyrene and benzo[*ghi*]perylene embedded in ammonia−ice become anionic when exposed to Lyman-α irradiation.[11] The formation of anionic PAHs becomes more prevalent as the ratio of ammonia to water in mixed ices increases. Cuylle *et al.* hypothesized that an electron can be transferred to the PAH through ammonia-related photoproducts, and therefore, anionic PAHs are formed. They did, however, not provide experimental evidence for how this process occurs.

The purpose of our study is to achieve an understanding of the underlying physical factors responsible for the observation that upon VUV irradiation, the PAHs in water−ice turn into their radical cations, whereas the PAHs in ammonia−ice rather transform into the corresponding radical anions. Under interstellar and laboratory conditions, PAHs are fully surrounded by matrix molecules. Herein, we aim at disentangling the origin of the observed phenomena from other bulk effects and investigate if, already at the level of the interaction between a single representative PAH and a single matrix molecule,[12] the two opposite tendencies can be recovered and related to a causal physical mechanism.

To understand the effect of the matrix on the photochemical behavior of the PAH in its essence, we need to go back to the fundamental difference in the interaction between one PAH molecule and one water *versus* one ammonia molecule. We first quantum-chemically analyze the fundamental differences between the electronic structures of water and ammonia in relation to those of three representative PAHs, benzene (**Ben**, C_6H_6), pyrene (**Py**, $C_{16}H_{10}$), and benzo[*ghi*]perylene (**BgP**, $C_{22}H_{12}$), using Kohn−Sham molecular orbital (MO) theory, as contained in Kohn−Sham density functional theory (DFT). Second, we analyze how these differences affect the nature of the PAH−water *versus* PAH−ammonia interaction with respect to the MO electronic spectra of the resulting PAH−matrix complexes and the associated potential ionization routes. Third, we compute the actual excitations and their oscillator strength using time-dependent DFT (TDDFT).

Here, we anticipate that we find fundamental differences between water and ammonia molecules that translate into opposite charge-transfer excitations in the corresponding complexes with PAHs, leading preferentially to PAH-to-water excitation (*i.e.*, PAH cation formation in the case of water) and ammonia-to-PAH excitation (*i.e.*, PAH anion formation in the case of ammonia).

2. COMPUTATIONAL DETAILS

2.1. General Procedure. Calculations were carried out with the Amsterdam Density Functional (ADF) program, version 2013.01.[13] The generalized gradient approximation functional BLYP was employed to find the equilibrium structures of all species using the basis set TZ2P, a small frozen core, and Grimme's DFT-D3 correction with Becke−Johnson (BJ) damping to correct for dispersion effects.[14] The TZ2P basis set is of valence triple-ζ quality and has been augmented by two polarization functions.[15] This basis set is known from previous work to yield relatively small basis-set superposition errors that can be safely neglected; see ref 15b. Scalar relativistic corrections were included using the zeroth-order regular approximation (ZORA) to allow for the possible expansion of this work in the future.[16,17] Numerical integration was performed with the Becke grid set to "verygood".[18] All geometry optimizations were performed in the gas phase and without imposing geometric constraints. The equilibrium geometries were confirmed to be in a (local) minimum-energy state using vibrational frequency analyses (*i.e.*, no imaginary frequencies were found).

2.2. Fock Matrix-Symmetrized Fragment Orbitals (FMATSFOs). In the ADF program, the electronic structure of molecular systems, such as our PAH−matrix complexes, can be analyzed in terms of the interaction between two meaningfully chosen fragments and the bonding mechanism between the corresponding fragment MOs. The effective orbital energies of fragments can and, in general, do change once these fragments are at their positions in the final complex and experience each other's electrostatic potential.[19,20] Often, but not always, the effective fragment MO energies are stabilized when they are exposed to the potential of the other fragment. Note that this is the actual starting situation from which orbital interactions take place. These shifted effective fragment orbital energies can be computed in ADF using the keyword FMATSFO.[19]

2.3. TDDFT Computations. Possible charge-transfer excitations between the PAHs and matrix molecules were investigated using TDDFT.[21] All optically allowed (*i.e.*, singlet−singlet) vertical excitations were calculated for the PAH−water and the PAH−ammonia complexes. The range-separated functional CAMY-B3LYP was used, along with a TZ2P basis set.[22] Relativistic effects were accounted for using ZORA.[16,17] The CAMY-B3LYP functional has shown to provide accurate results for charge-transfer excitations in naphthalene derivatives and is therefore a suitable functional to study the PAHs in this work.[23] For more detailed information on the CAMY-B3LYP functional, we refer to ref 22b.

3. RESULTS AND DISCUSSION

3.1. MO Analysis of Ammonia, Water, and PAHs. Understanding of the ionization pathways of PAHs in water and ammonia−ice starts with the quantum chemical analysis of the electronic structure of the two different-matrix molecules (H_2O and NH_3). In this analysis, we focus on the highest occupied MOs (HOMOs) and lowest unoccupied MOs (LUMOs) in particular since these levels are most likely involved in electronic excitations. Figure 1 shows the optimized geometries and the HOMO and LUMO orbitals and corresponding energies of water and ammonia.

The HOMO of ammonia ($HOMO_A$) is at a relatively high energy (−6.1 eV) compared to the HOMO of water ($HOMO_W$, −7.2 eV), resulting in an energy difference between the two HOMOs of 1.1 eV. These HOMOs represent the lone pair (LP) of ammonia and the highest-energy LP of water (the HOMO − 1_W of water, i.e., the other LP, lies at −9.2 eV). In contrast to the HOMOs, the energy difference between the LUMOs of the two matrix molecules is relatively small, only 0.4 eV, where the LUMO of ammonia lies at −0.5 eV and the LUMO of water at −0.9 eV. Qualitatively, similar results are obtained when the water and ammonia molecule are

https://doi.org/10.1021/acsearthspacechem.1c00433
ACS Earth Space Chem. 2022, 6, 766−774

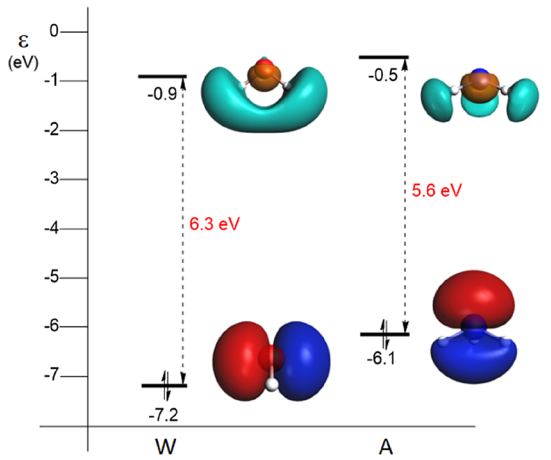

Figure 1. HOMO and LUMO energy levels (in eV) of water (**W**) and ammonia (**A**), along with their isosurfaces (at 0.05 au), calculated at the ZORA-BLYP-D3(BJ)/TZ2P level of theory in the gas phase.

in a medium of other like molecules (the HOMO−LUMO gaps increase by *ca.* 0.5 eV; see Figure S1).

Next, we compare the relative positioning of the HOMO and LUMO of ammonia and water to the frontier MOs of pyrene (**Py**) and benzo[*ghi*]perylene (**BgP**), which are representative for the PAHs used in the experiments by Cuylle *et al.* [see Figure 2 for the energy levels of **Py**, **W**, and **A** (left) and **BgP**, **W**, and **A** (right)].[11] The HOMO and LUMO have π- and π^*-like characters, respectively, for both **Py** and **BgP**. The smallest intermolecular HOMO−LUMO gap with regard to water and ammonia is encircled in red (see Figure 2). The energy gap between the $HOMO_A$ and the $LUMO_{PAH}$ is smaller than the energy gap between the $HOMO_W$ and the $LUMO_{PAH}$ due to the higher-lying $HOMO_A$. For ammonia, it amounts to 3.7 and 3.5 eV between $HOMO_A$ and, respectively, the $LUMO_{Py}$ and $LUMO_{BgP}$. For water, the values are 4.8 and 4.6 eV between the $HOMO_W$ and, respectively, the LUMOs of **Py** and **BgP**. The energy differences between the HOMO of the PAHs and the LUMOs of ammonia and water are less pronounced as the LUMOs of the matrix molecules differ less. The smallest energy gap here is found between the $HOMO_{PAH}$ and the $LUMO_W$, being 4.1 and 4.0 eV for **Py** and **BgP**, respectively (see also Figure 2).

Let us consider an electron transfer in these model systems assuming that the electron transfer occurs *via* the smallest energy gap (see encircled gaps in Figure 2). In a PAH−water complex, the electron is excited over the smaller energy gap from the PAH to water (4.1 and 4.0 eV for **Py** and **BgP**) than from water to the PAH (4.8 and 4.6 eV for **Py** and **BgP**). This suggests that it is more likely to form cationic PAHs in a PAH−water complex than the anionic species. In the case of PAH−ammonia complexes, it is the other way around. The electron is more easily excited over the smaller energy gap from ammonia to the PAH (3.7 and 3.5 eV for **Py** and **BgP**, respectively) than from the PAH to ammonia (4.5 and 4.4 eV for **Py** and **BgP**, respectively). Here, the suggestion is that it is more likely to form anionic PAHs in a PAH−ammonia complex than cationic PAHs. These findings are consistent with the observations of Cuylle *et al.* in their *in situ* experiments.[11]

The ground-state energetics of the individual molecules give a good indication of the electronic differences between ammonia and water and how the relative HOMO and LUMO energies of ammonia, water, and the PAHs are responsible for the size of the intermolecular energy gaps. Note, however, that this simplified picture is an incomplete representation as charge-transfer excitations that occur in interstellar ices involve PAHs embedded in them, thus interacting with ammonia and water. The individual ground-state HOMO−LUMO levels do not take into account any change in the MOs as a result of the interaction between the PAHs and the matrix molecules. This coupling or mixing of the PAH levels with the matrix electronic structure is crucial for

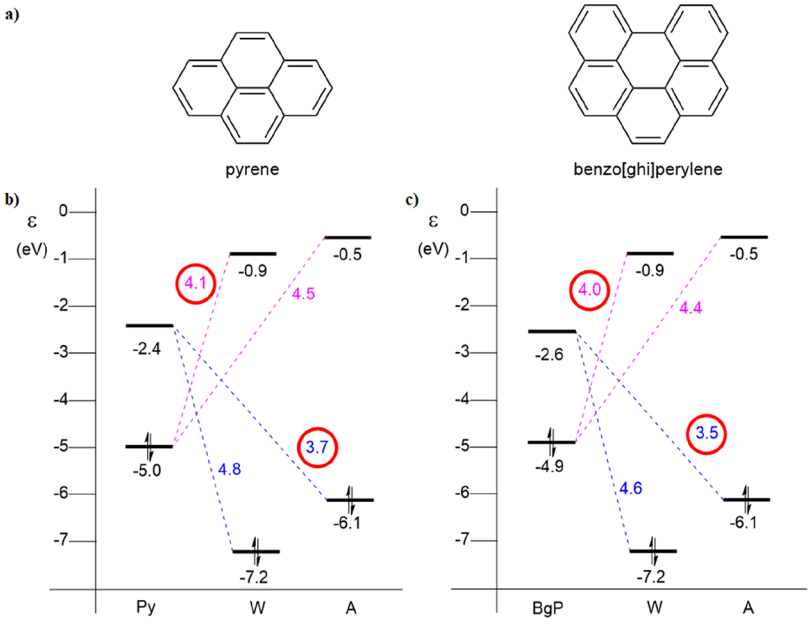

Figure 2. (a) Molecular structures of pyrene (**Py**) and benzo[*ghi*]perylene (**BgP**). (b) HOMO−LUMO energy levels (in eV) of water (**W**) and ammonia (**A**) compared to **Py** and (c) **BgP**, calculated at the ZORA-BLYP-D3(BJ)/TZ2P level of theory in the gas phase. The smallest intermolecular energy gaps are encircled in red.

https://doi.org/10.1021/acsearthspacechem.1c00433
ACS Earth Space Chem. 2022, 6, 766−774

understanding the actual factors determining the transition probability for PAHs in water−ice *versus* that of PAHs in ammonia−ice (*vide infra*).

3.2. MO Interaction Diagrams of PAH−Matrix Complexes. In the previous section, we analyzed the ground-state frontier MOs of the individual PAH, water, and ammonia molecules. For a basic analysis of the MOs of small molecules, we refer the reader to the book "Orbital Interactions in Chemistry" by T. A. Albright *et al.*, see ref 24. Next, we quantify the interactions in the PAH−ammonia and PAH−water complexes to see how the HOMO−LUMO levels change as a result of the interaction. Interacting PAH−matrix complexes were created by placing a single matrix molecule above the π-electronic system of the aromatic rings and subsequently optimizing the complex (see Figure 3). For each of the final six complexes (labeled **BenW**, **BenA**, **PyW**, **PyA**, **BgPW**, and **BgPA**), energy minima were found. In the optimized geometries, the ammonia and water molecules direct the N−H or O−H bond(s) toward the π-system of the PAH, see Figure 3. The Cartesian coordinates of the optimized PAH−matrix complexes can be found in the Supporting Information. Note that we find several local minima for each PAH−matrix combination. These complexes are very similar, both energetically and in terms of their interaction mechanism but only differ in the exact position at which the matrix molecule binds to the π-system of the PAH. Herein, we highlight one of the obtained complexes per PAH−matrix combination that clearly demonstrates the fundamental differences between the PAH−ammonia and PAH−water complexes. For the geometries of the other computed PAH−matrix complex minima, the reader is referred to Figure S3.

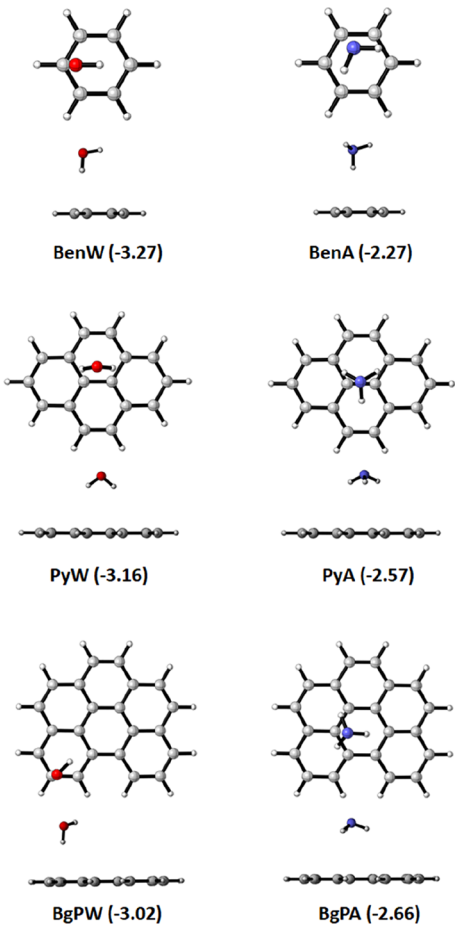

Figure 3. Optimized PAH−matrix complexes (top view and side view) with the calculated bond energy shown in parentheses in kcal mol^{-1}, calculated at the ZORA-CAMY-B3LYP-D3(BJ)/TZ2P//ZORA-BLYP-D3(BJ)/TZ2P level of theory. For the bond energy calculated fully with ZORA-BLYP-D3(BJ)/TZ2P, see Figure S2.

The interaction between the PAH and matrix molecule when forming the PAH−matrix complexes is small, with the bond energies ranging between −2.27 and −3.27 kcal mol^{-1}, which can be considered as a weak N(H)···π or O(H)···π hydrogen bond interaction. In general, the bond energy for the PAH−water complexes (−3.02 to −3.27 kcal mol^{-1}) is more stabilizing than that for the PAH−ammonia complexes (−2.27 to −2.66 kcal mol^{-1}).

Next, the interaction between the PAH and the matrix molecules in the PAH−matrix complexes is further investigated. The **Py**−matrix complexes are highlighted here to provide general insights on the PAH−matrix interaction as similar results were found for the **Ben**−matrix and **BgP**−matrix complexes. Additional orbital interaction figures for the **Ben**−matrix, **Py**−matrix, and **BgP**−matrix complexes can be found in Figures S4−S9 of the Supporting Information.

The interaction between the occupied MOs of pyrene and the matrix molecules water and ammonia is given in Figure 4. The extent of mixing between the PAH and matrix-molecule orbitals is determined not only by the differences in energy between the orbitals of the PAHs and the matrix molecules but also for an important extent by the orbital overlap. Now, we first inspect how much the extent of mixing is in the case of a water and an ammonia matrix. For the **PyW** complex (Figure 4a), there is very little-to-no mixing that occurs in the occupied MOs of the **PyW** complex, with roughly 98% of the HOMO − 2_{PyW} originating from the HOMO − 2_{Py}, 100% of the HOMO − 3_{PyW} originating from the HOMO − 3_{Py}, and 98% of the HOMO − 4_{PyW} originating from the $HOMO_W$. Thus, the occupied π-orbitals of pyrene (HOMO − 2_{Py} and HOMO − 3_{Py}) and the LP of water ($HOMO_W$) mix minimally and remain mostly localized on the original fragments.

In contrast, the LP of ammonia ($HOMO_A$) and a π-orbital of pyrene (HOMO − 2_{Py}) mix strongly in the **PyA** complex (Figure 4b). Two delocalized MOs (HOMO − 2_{PyA} and HOMO − 3_{PyA}) are formed, with roughly 14% of the total MO originating from one monomer while the remaining 85−86% originating from the other monomer (see Figure 4b). It is a manifestation of the Pauli exclusion principle due to the overlap between occupied orbitals of both monomers (see Tables S1 and S2). The HOMO − 3_{PyA} is a bonding combination, and the HOMO − 2_{PyA} is an antibonding combination between the HOMO − 2_{Py} and the $HOMO_A$. This difference in interaction between the PAH−water and PAH−ammonia complexes can be attributed to the HOMO energies of the two matrix molecules and orbital overlap between HOMO of the matrix molecules (ammonia or water) and π-orbitals of the PAH.

Now, we return to the rationale behind the stronger PAH−matrix orbital mixing in the case of ammonia compared to water. The amount of mixing between an orbital on one monomer and an orbital on the other monomer is approximately proportional to the overlap between the two orbitals on both monomers S (more precisely, it is proportional to the matrix element between the two orbitals) and inversely proportional to the energy difference between those

https://doi.org/10.1021/acsearthspacechem.1c00433
ACS Earth Space Chem. 2022, 6, 766−774

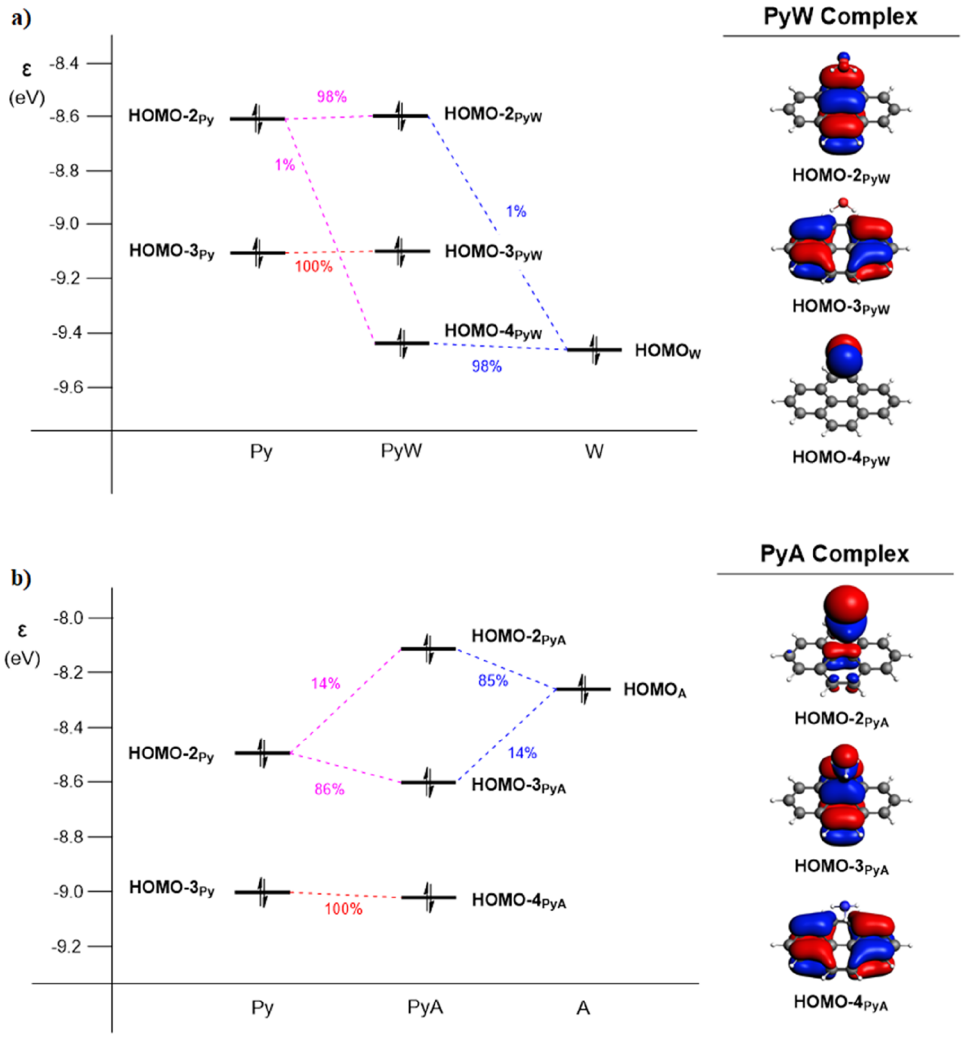

Figure 4. Orbital interaction diagram of occupied fragment MOs (FMOs) of (a) **PyA** and (b) **PyW**, with FMO contributions (in %) and visualization of the overall complex MOs (isosurface at 0.03 au), calculated at the ZORA-CAMY-B3LYP/TZ2P level of theory. The FMO energies are calculated in the field of the other fragment, as described in Computational Details Section 2.2, and reported in Table S3. For a full description of the occupied MOs, see Figures S6 and S7.

orbitals, $\Delta\varepsilon$. The absolute energy gap between the $HOMO_A$ of ammonia and the HOMO $-$ 2_{Py} (0.24 eV) is much smaller than the gap between the $HOMO_W$ of water and the HOMO $-$ 2_{Py} (0.84 eV), as can be seen in Figure 4. Furthermore, the spatial orientation of the LP of ammonia relative to the PAH allows for better orbital overlap with the PAH MOs in comparison to water (see also Figures 1 and 3). The reason for this is that the ammonia LP is essentially the nitrogen $2p_z$ (with a slight admixture of hydrogen 1s character), and due to ammonia's trigonal pyramidal geometry, as it points with its N$-$H bond(s) to the PAH, the LP also points directly to the π-system of the PAH and, thus, overlaps well. In contrast, the oxygen 2p-type LP is arranged parallel to the PAH surface as the water molecule points with its O$-$H bond(s) to the PAH (see also Figures 1 and 3). This orbital does not point with a lobe toward the PAH and therefore has a smaller overlap with the π-system. For example, in the **PyA** complex, the orbital overlap between the LP of ammonia ($HOMO_A$) and the π-orbital of pyrene (HOMO $-$ 2_{Py}) is larger (S = 0.0266) than the overlap between the LP of water ($HOMO_W$) and the π-orbital of pyrene (HOMO $-$ 2_{Py}) in the **PyW** complex, which is only 0.0175 (see Table S2). The orbital overlap between the $HOMO_W$ and HOMO $-$ 3_{Py} is even 1 order of magnitude smaller (S = 0.0017). These smaller orbital overlaps explain why the MOs of pyrene do not mix significantly with the $HOMO_W$.

The strong mixing in the **PyA** complex and the poor mixing in the **PyW** complex is a clear fundamental difference between these two complexes. As will be shown in the following section, the formation of these mixed PAH$-$ammonia MOs plays an important role in the available charge-transfer pathways.

3.3. Charge-Transfer Excitations in Interacting PAH$-$Matrix Complexes. In this section, we analyze the possible charge-transfer excitation pathways in the PAH$-$matrix complexes (Figure 3) using TDDFT calculations. All charge-transfer excitations below 10.2 eV (Lyman-α radiation) with an oscillator strength greater than 0.2 are considered in the exploration of the possibility of charge transfer upon VUV irradiation. The calculated charge-transfer excitations are reported in Table 1 for the complexes of Figure 3. See Table S4 and Figure S11 for the charge-transfer excitations of other local minima of these PAH$-$matrix complexes. In this section, we focus mostly on the **Py**$-$matrix complexes as these complexes clearly explain the difference between PAH$-$water

https://doi.org/10.1021/acsearthspacechem.1c00433
ACS Earth Space Chem. 2022, 6, 766−774

Table 1. Charge-Transfer Excitations (in eV) in PAH−Matrix Complexes Calculated at the ZORA-CAMY-B3LYP/TZ2P Level of Theory[a]

complexes	transition (eV)	oscillator strength	weight (%)	from the MO (complex)	to the MO (complex)	character of charge-transfer direction
BenW	7.09	0.443	18.9	HOMO − 1_{BenW}	LUMO + 2_{BenW}	$\pi_{PAH} \rightarrow \sigma^*_{PAH} + \sigma^*_{H_2O}$
BenA	7.11	0.610	26.4	HOMO − 2_{BenA}	LUMO + 1_{BenA}	π_{PAH} & $LP_{NH_3} \rightarrow \pi^*_{PAH}$
			20.3	$HOMO_{BenA}$	LUMO + 1_{BenA}	π_{PAH} & $LP_{NH_3} \rightarrow \pi^*_{PAH}$
	7.10	0.547	25.7	HOMO − 2_{BenA}	$LUMO_{BenA}$	π_{PAH} & $LP_{NH_3} \rightarrow \pi^*_{PAH}$
			19.3	$HOMO_{BenA}$	$LUMO_{BenA}$	π_{PAH} & $LP_{NH_3} \rightarrow \pi^*_{PAH}$
PyW	7.35	0.599	12.2	HOMO − 2_{PyW}	LUMO + 4_{PyW}	$\pi_{PAH} \rightarrow \sigma^*_{PAH} + \sigma^*_{H_2O}$
	6.70	0.544	29.3	HOMO − 1_{PyW}	LUMO + 4_{PyW}	$\pi_{PAH} \rightarrow \sigma^*_{PAH} + \sigma^*_{H_2O}$
	7.21	0.418	5.3	HOMO − 2_{PyW}	LUMO + 4_{PyW}	$\pi_{PAH} \rightarrow \sigma^*_{PAH} + \sigma^*_{H_2O}$
	6.66	0.259	57	HOMO − 1_{PyW}	LUMO + 4_{PyW}	$\pi_{PAH} \rightarrow \sigma^*_{PAH} + \sigma^*_{H_2O}$
PyA	7.30	0.780	62.3	HOMO − 3_{PyA}	LUMO + 3_{PyA}	π_{PAH} & $LP_{NH_3} \rightarrow \pi^*_{PAH}$
	6.76	0.675	85.9	HOMO − 3_{PyA}	LUMO + 2_{PyA}	π_{PAH} & $LP_{NH_3} \rightarrow \pi^*_{PAH}$
BgPW	6.53	1.053	5.7	HOMO − 1_{BgPW}	LUMO + 5_{BgPW}	$\pi_{PAH} \rightarrow \sigma^*_{PAH} + \sigma^*_{H_2O}$
			3.7	$HOMO_{BgPW}$	LUMO + 8_{BgPW}	$\pi_{PAH} \rightarrow \sigma^*_{PAH} + \sigma^*_{H_2O}$
BgPA	6.95	0.742	31.0	HOMO − 3_{BgPA}	LUMO + 4_{BgPA}	π_{PAH} & $LP_{NH_3} \rightarrow \pi^*_{PAH}$
	6.58	0.443	26.7	HOMO − 3_{BgPA}	LUMO + 3_{BgPA}	π_{PAH} & $LP_{NH_3} \rightarrow \pi^*_{PAH}$
			8.4	HOMO − 2_{BgPA}	LUMO + 3_{BgPA}	π_{PAH} & $LP_{NH_3} \rightarrow \pi^*_{PAH}$
	6.46	0.353	38.6	HOMO − 2_{BgPA}	LUMO + 3_{BgPA}	π_{PAH} & $LP_{NH_3} \rightarrow \pi^*_{PAH}$
	6.60	0.268	15.1	HOMO − 3_{BgPA}	LUMO + 3_{BgPA}	π_{PAH} & $LP_{NH_3} \rightarrow \pi^*_{PAH}$
	6.13	0.205	23.3	HOMO − 2_{BgPA}	LUMO + 2_{BgPA}	π_{PAH} & $LP_{NH_3} \rightarrow \pi^*_{PAH}$

[a]Lone pairs are abbreviated as LP. The MOs involved in the charge-transfer excitations (columns 5 and 6) can be found in Figure 5.

and PAH−ammonia complexes. All relevant MOs involved in the **Py**−matrix excitations are shown in Figure 5. The MOs of the **Ben**−matrix and **BgP**−matrix complexes can be found in Figure S10.

In the **PyW** complex, charge-transfer excitations can occur from the localized π-orbitals of pyrene (HOMO − 1_{PyW} or HOMO − 2_{PyW}) to a delocalized unoccupied MO consisting of the mixed PAH−water σ*-orbital with a large coefficient on the water molecule (LUMO + 4_{PyW}), see Figure 5. This direction of charge-transfer excitations suggests that pyrene donates electronic density to water and therefore can become positively charged upon irradiation.

Interestingly, the direction of charge-transfer excitations in the **PyA** complex is different from the water-embedded variant **PyW**. In the **PyA** complex, charge-transfer excitations are observed from a mixed MO with ammonia and pyrene π-orbital character (HOMO − 3_{PyA}) to two different unoccupied MOs with a π*-like character localized on the pyrene molecule (LUMO + 2_{PyA} or LUMO + 3_{PyA}), see Figure 5. This direction of charge-transfer excitation leads to a shift of charge density from the occupied mixed MO of the complex toward the unoccupied orbitals of pyrene and indicates a net electronic density flow from ammonia to pyrene, leading to a negatively charged PAH upon irradiation. These results on the dimers of PAH−water and PAH−ammonia show the same trends as the experimental findings by Cuylle *et al.*, who reported the formation of anionic PAHs in an ammonia matrix, while cationic PAHs were formed in a water matrix.[11]

The results for the **BenW** and **BgPW** complexes are similar to those for the **PyW** complex: charge-transfer excitations are observed from localized π-orbitals (HOMO − 1_{BenW} for **BenW** and $HOMO_{BgPW}$ or HOMO − 1_{BgPW} for **BgPW**) toward mixed PAH−water σ*-MOs (LUMO + 2_{BenW} for **BenW** and LUMO + 5_{BgPW} or LUMO + 8_{BgPW} for **BgPW**). This suggests the formation of cationic PAH radicals upon the irradiation of PAH−water complexes. For the **BenA** and **BgPA** complexes, all observed charge-transfer excitations originate from mixed MOs of the LP of ammonia and the π-orbitals of the aromatic molecule ($HOMO_{BenA}$ or HOMO − 2_{BenA} for **BenA** and HOMO − 2_{BgPA} or HOMO − 3_{BgPA} for **BgPA**) toward localized π*-orbitals of the aromatic molecule ($LUMO_{BenA}$ or LUMO + 1_{BenA} for **BenA** and LUMO + 2_{BgPA}, LUMO + 3_{BgPA}, or LUMO + 4_{BgPA} for **BgPA**). Accordingly, this direction of charge transfer suggests the formation of anionic PAH radicals. These results are recovered in all other PAH−ammonia complexes, which all go with predominant ammonia to PAH excitations. In the case of other PAH−water complexes, the situation is not always that consistent, and in some cases, besides PAH-to-water excitations, there also exist water-to-PAH excitations.

In the study by Cuylle *et al.*, it was shown that changing the ratio of water/ammonia in the ice matrix gives rise to a turning point in the ionization direction, that is, raising the ratio water/ammonia led to the formation of cationic PAHs over anionic PAHs. Our TDDFT findings nicely explain this phenomenon: raising the ratio water/ammonia implies strengthening the mechanism that leads to PAH cation formation while lowering the ratio water/ammonia corresponds to reinforcing the mechanism of PAH anion formation. Note however that our archetypal model systems do not allow for a prediction of the water/ammonia ratio at which the turning point occurs.

4. CONCLUSIONS

We have quantum-chemically developed a rationale for the experimental observation that water−ice-embedded PAHs become cationic when exposed to high-energy irradiation,

https://doi.org/10.1021/acsearthspacechem.1c00433
ACS Earth Space Chem. 2022, 6, 766−774

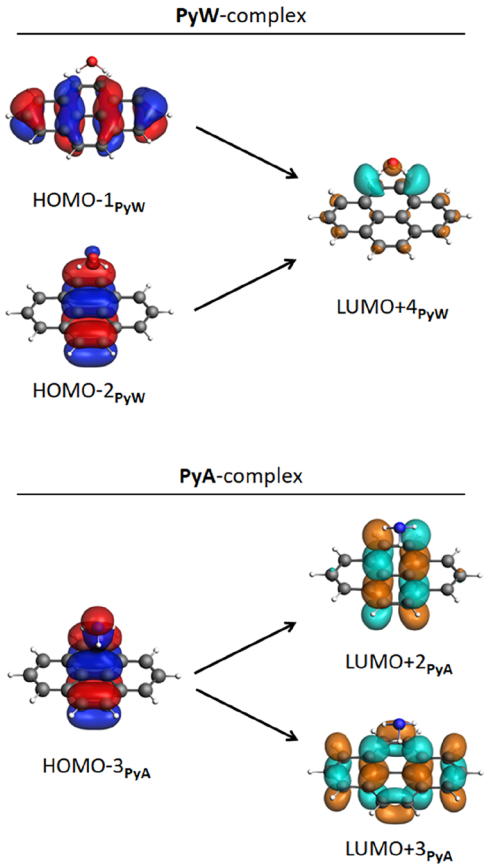

Figure 5. Relevant MOs involved in charge-transfer excitations for **PyW** (top) and **PyA** (bottom) with isosurfaces (at 0.03 au) calculated at the CAMY-B3LYP/TZ2P level of theory. Occupied MOs are red and blue, while unoccupied MOs are cyan and orange. Optimized structures can be found in Figure 3. The situation is similar for **BenW**, **BenA**, **BgPW**, and **BgPA**; see Figures S12 and S13.

whereas ammonia–ice-embedded PAHs lead to the formation of anionic PAH photoproducts. Interestingly, this turns out to be not so much an average medium effect but rather the consequence of discrete quantum chemical interactions that are already effective upon bonding one matrix molecule in PAH–water and PAH–ammonia complexes.

Our analyses, based on Kohn–Sham MO theory and TDDFT, reveal that the nitrogen LP-type HOMO of ammonia is optimally oriented toward the aromatic π-system as this matrix molecule binds with its N–H bond(s) to the PAH. This orientation, and the relatively high energy of the ammonia LP HOMO, guarantees good overlap and strong mixing between occupied ammonia and PAH orbitals. Indeed, our TDDFT analyses confirm that excitations from occupied orbitals of the PAH–ammonia complex have a strong component of charge transfer from the ammonia matrix into virtual orbitals that are largely on the PAH. In other words, this generates PAH radical anions.

At variance, the oxygen LP-type HOMO of water is suboptimally oriented, namely, in parallel to the aromatic π-system as this matrix molecule binds with its O–H bond(s) to the PAH. This orientation, and the somewhat lower energy of the water LP HOMO, impair the buildup of overlap and the mixing between occupied water and PAH orbitals. This yields a situation in which excitations take place from occupied orbitals that remain mainly localized on the PAH into virtuals with water and PAH character, as perceived from TDDFT analyses. This comes down to generating PAH radical cations.

■ ASSOCIATED CONTENT

Supporting Information

The Supporting Information is available free of charge at https://pubs.acs.org/doi/10.1021/acsearthspacechem.1c00433.

Bond energies, orbital interaction diagrams, and MOs of the PAH–matrix complexes and energy decomposition analysis, TDDFT results, and Cartesian coordinates of the optimized PAH–matrix complexes (PDF)

■ AUTHOR INFORMATION

Corresponding Authors

F. Matthias Bickelhaupt − *Department of Theoretical Chemistry, Amsterdam Institute of Molecular and Life Sciences (AIMMS), Amsterdam Center for Multiscale Modeling (ACMM), Vrije Universiteit Amsterdam, 1081 HV Amsterdam, The Netherlands; Institute for Molecules and Materials (IMM), Radboud University, 6525 AJ Nijmegen, The Netherlands;* orcid.org/0000-0003-4655-7747; Email: f.m.bickelhaupt@vu.nl

Célia Fonseca Guerra − *Department of Theoretical Chemistry, Amsterdam Institute of Molecular and Life Sciences (AIMMS), Amsterdam Center for Multiscale Modeling (ACMM), Vrije Universiteit Amsterdam, 1081 HV Amsterdam, The Netherlands; Leiden Institute of Chemistry, Gorlaeus Laboratories, Leiden University, 2333 CC Leiden, The Netherlands;* orcid.org/0000-0002-2973-5321; Email: c.fonsecaguerra@vu.nl

Authors

Stephanie ten Brinck − *Department of Theoretical Chemistry, Amsterdam Institute of Molecular and Life Sciences (AIMMS), Amsterdam Center for Multiscale Modeling (ACMM), Vrije Universiteit Amsterdam, 1081 HV Amsterdam, The Netherlands*

Celine Nieuwland − *Department of Theoretical Chemistry, Amsterdam Institute of Molecular and Life Sciences (AIMMS), Amsterdam Center for Multiscale Modeling (ACMM), Vrije Universiteit Amsterdam, 1081 HV Amsterdam, The Netherlands;* orcid.org/0000-0002-5855-4386

Angela van der Werf − *Department of Theoretical Chemistry, Amsterdam Institute of Molecular and Life Sciences (AIMMS), Amsterdam Center for Multiscale Modeling (ACMM), Vrije Universiteit Amsterdam, 1081 HV Amsterdam, The Netherlands*

Richard M. P. Veenboer − *Department of Theoretical Chemistry, Amsterdam Institute of Molecular and Life Sciences (AIMMS), Amsterdam Center for Multiscale Modeling (ACMM), Vrije Universiteit Amsterdam, 1081 HV Amsterdam, The Netherlands;* orcid.org/0000-0002-4878-580X

Harold Linnartz − *Laboratory for Astrophysics, Leiden Observatory, Leiden University, 2300 RA Leiden, The Netherlands;* orcid.org/0000-0002-8322-3538

Complete contact information is available at: https://pubs.acs.org/10.1021/acsearthspacechem.1c00433

https://doi.org/10.1021/acsearthspacechem.1c00433
ACS Earth Space Chem. 2022, 6, 766−774

Notes

The authors declare no competing financial interest.

■ ACKNOWLEDGMENTS

The authors thank Louis Allamandola and A. (Xander) G. G. M. Tielens for the useful discussions, which contributed to the start of this research and the shaping of the research question. The authors thank the Netherlands Organization for Scientific Research (NWO) and the Dutch Astrochemistry Network (DAN) for financial support.

■ REFERENCES

(1) (a) Gillett, F. C.; Forrest, W. J.; Merrill, K. M. 8-13-Micron Spectra of NGC 7027, BD+30°3639, and NGC 6572. *Astrophys. J.* **1973**, *183*, 87−93. (b) Allamandola, L. J.; Tielens, A. G. G. M.; Barker, J. R. Polycyclic Aromatic Hydrocarbons and the Unidentified Infrared: Auto Exhaust Along the Milky Way! *Astrophys. J.* **1985**, *290*, L25−L28. (c) Allamandola, L. J.; Tielens, G. G. M.; Barker, J. R. Interstellar Polycyclic Aromatic Hydrocarbons: The Infrared Emission Bands, The Excitation/Emission Mechanism, and the Astrophysical Implications. *Astrophys. J., Suppl. Ser.* **1989**, *71*, 733−775. (d) Allamandola, L. J.; Sandford, S. A.; Hudgins, D. M.; Witteborn, F. C. Airborne and Laboratory Studies of Interstellar PAHs. *ASP Conf. Ser.* **1995**, *73*, 23−32. (e) Leger, A.; Puget, J. L. Identification of the "Unidentified" IR Emission Features of Interstellar Dust? *Astron. Astrophys.* **1984**, *137*, L5−L8. (f) Joblin, C.; Tielens, A. G. G. M. PAHs and the Universe: A Symposium to Celebrate the 25th Anniversary of the PAH Hypothesis. *EAS Publ. Ser.* **2011**, *46*, 1−468. (g) Tielens, A. G. G. M. Interstellar Polycyclic Aromatic Hydrocarbon Molecules. *Annu. Rev. Astron. Astrophys.* **2008**, *46*, 289−337. (h) Puget, J. L.; Léger, A. A New Component of the Interstellar Matter: Small Grains and Large Aromatic Molecules. *Annu. Rev. Astron. Astrophys.* **1989**, *27*, 161−198. (i) Pierrefixe, S. C. A. H.; Bickelhaupt, F. M. Aromaticity. Molecular Orbital Picture of an Intuitive Concept. *Chem. Eur. J.* **2007**, *13*, 6321−6328.

(2) Duley, W. W.; Williams, D. A. The Infrared Spectrum of Interstellar Dust: Surface Functional Groups on Carbon. *Mon. Not. R. Astron. Soc.* **1981**, *196*, 269−274.

(3) (a) Cernicharo, J.; Agúndez, M.; Kaiser, R. I.; Cabezas, C.; Tercero, B.; Marcelino, N.; Pardo, J. R.; de Vicente, P. Discovery of benzyne, *o*-C_6H_4, in TMC-1 with the QUIJOTE line survey. *Astron. Astrophys.* **2021**, *652*, L9. (b) Cernicharo, J.; Agúndez, M.; Cabezas, C.; Tercero, B.; Marcelino, N.; Pardo, J. R.; de Vicente, P. Pure hydrocarbon cycles in TMC-1: Discovery of ethynyl cyclopropenylidene, cyclopentadiene and indene. *Astron. Astrophys.* **2021**, *649*, L15. (c) McGuire, B. A.; Burkhardt, A. M.; Kalenskii, S.; Shingledecker, C. N.; Remijan, A. J.; Herbst, E.; McCarthy, M. C. Detection of the aromatic molecule benzonitrile (*c*-C_6H_5CN) in the interstellar medium. *Science* **2018**, *359*, 202−205.

(4) (a) Pontoppidan, K. M.; van Dishoeck, E. F.; Dartois, E. Mapping ices in protostellar environments on 1000 AU scales. *Astron. Astrophys.* **2004**, *426*, 925−940. (b) Öberg, K. I.; van Dishoeck, E. F.; Linnartz, H.; Andersson, S. The effect of H_2O on ice photochemistry. *Astrophys. J.* **2010**, *718*, 832−840.

(5) (a) Boogert, A. C. A.; Gerakines, P. A.; Whittet, D. C. B. Observations of the Icy Universe. *Annu. Rev. Astron. Astrophys.* **2015**, *53*, 541−581. (b) Linnartz, H.; Ioppolo, S.; Fedoseev, G. Atom addition reactions in interstellar ice analogues. *Int. Rev. Phys. Chem.* **2015**, *34*, 205−237. (c) Ioppolo, S.; Cuppen, H. M.; Romanzin, C.; van Dishoeck, E. F.; Linnartz, H. Water formation at low temperatures by surface O2 hydrogenation I: characterization of ice penetration. *Phys. Chem. Chem. Phys.* **2010**, *12*, 12065−12076. (d) Fedoseev, G.; Ioppolo, S.; Zhao, D.; Lamberts, T.; Linnartz, H. Low-temperature surface formation of NH3 and HNCO: hydrogenation of nitrogen atoms in CO-rich interstellar ice analogues. *Mon. Not. R. Astron. Soc.* **2015**, *446*, 439−448.

(6) Bottinelli, S.; Boogert, A. C. A.; Bouwman, J.; Beckwith, M.; van Dishoeck, E. F.; Öberg, K. I.; Pontoppidan, K. M.; Linnartz, H.; Blake, G. A.; Evans, N. J.; Lahuis, F. The c2d Spitzer Spectroscopic Survey of Ices Around Low-mass Young Stellar Objects. IV. NH_3 and CH_3OH. *Astrophys. J.* **2010**, *718*, 1100−1117.

(7) (a) Bernstein, M. P.; Sandford, S. A.; Allamandola, L. J.; Gillette, J. S.; Clemett, S. J.; Zare, R. N. UV Irradiation of Polycyclic Aromatic Hydrocarbons in Ices: Production of Alcohols, Quinones, and Ethers. *Science* **1999**, *283*, 1135−1138. (b) Bernstein, M. P.; Dworkin, J. P.; Sandford, S. A.; Cooper, G. W.; Allamandola, L. J. Racemic Amino Acids from the Ultraviolet Photolysis of Interstellar Ice Analogues. *Nature* **2002**, *416*, 401−403. (c) Gerakines, P. A.; Schutte, W. A.; Ehrenfreund, P. Ultraviolet Processing of Interstellar Ice Analogs. *Astron. Astrophys.* **1996**, *312*, 289−305. (d) Muñoz Caro, G. M.; Meierhenrich, U. J.; Schutte, W. A.; Barbier, B.; Arcones Segovia, A.; Rosenbauer, H.; Thiemann, W. H.-P.; Brack, A.; Greenberg, J. M. Amino Acids from Ultraviolet Irradiation of Interstellar Ice Analogues. *Nature* **2002**, *416*, 403−406. (e) Oba, Y.; Takano, Y.; Naraoka, H.; Watanabe, N.; Kouchi, A. Nucleobase Synthesis in Interstellar Ices. *Nat. Commun.* **2019**, *10*, 4413.

(8) (a) Gudipati, M. S.; Allamandola, L. J. Facile Generation and Storage of Polycyclic Aromatic Hydrocarbon Ions in Astrophysical Ices. *Astrophys. J.* **2003**, *596*, L195−L198. (b) Gudipati, M. S.; Allamandola, L. J. Unusual Stability of Polycyclic Aromatic Hydrocarbons Radical Cations in Amorphous Water Ices up to 120K: Astronomical Implications. *Astrophys. J.* **2006**, *638*, 286−292.

(9) Bouwman, J.; Cuppen, H. M.; Bakker, A.; Allamandola, L. J.; Linnartz, H. Photochemistry of the PAH Pyrene in Water Ice: The Case for Ion-Mediated Solid-State Astrochemistry. *Astron. Astrophys.* **2010**, *511*, A33.

(10) Kofman, V.; Witlox, M. J. A.; Bouwman, J.; ten Kate, I. L.; Linnartz, H. A multifunctional setup to record FTIR and UV-vis spectra of organic molecules and their photoproducts in astronomical ices. *Rev. Sci. Instrum.* **2018**, *89*, 053111.

(11) Cuylle, S. H.; Tenenbaum, E. D.; Bouwman, J.; Linnartz, H.; Allamandola, L. J. Lyα-Induced Charge Effects of Polycyclic Aromatic Hydrocarbons Embedded in Ammonia and Ammonia: Water Ice. *Mon. Not. R. Astron. Soc.* **2012**, *423*, 1825−1830.

(12) (a) Bickelhaupt, F. M.; Baerends, E. J.; Anibbering, N. M. M. The Effect of Microsolvation on E2 and S_N2 Reactions: Theoretical Study of the Model System F^- + C_2H_5F + *n* HF. *Chem.—Eur. J.* **1996**, *2*, 196−207. (b) Osuna, S.; Swart, M.; Baerends, E. J.; Bickelhaupt, F. M.; Solà, M. Homolytic versus heterolytic dissociation of alkalimetal halides: the effect of microsolvation. *ChemPhysChem* **2009**, *10*, 2955−2965.

(13) (a) te Velde, G.; Bickelhaupt, F. M.; Baerends, E. J.; Fonseca Guerra, C.; van Gisbergen, S. J. A.; Snijders, J. G.; Ziegler, T. Chemistry with ADF. *J. Comput. Chem.* **2001**, *22*, 931−967. (b) Fonseca Guerra, C.; Snijders, J. G.; te Velde, G.; Baerends, E. J. Towards an Order-N DFT Method. *Theor. Chem. Acc.* **1998**, *99*, 391−403. (c) *ADF2013, SCM, Theoretical Chemistry*; Vrije Universiteit: Amsterdam, The Netherlands. http://www.scm.com, 2013.

(14) (a) Grimme, S.; Antony, J.; Ehrlich, S.; Krieg, H. A Consistent and Accurate Ab Initio Parametrization of Density Functional Dispersion Correction (DFT-D) for the 94 Elements H-Pu. *J. Chem. Phys.* **2010**, *132*, 154104. (b) Grimme, S.; Ehrlich, S.; Goerigk, L. Effect of the Damping Function in Dispersion Corrected Density Functional Theory. *J. Comput. Chem.* **2011**, *32*, 1456−1465. (c) Johnson, E. R.; Becke, A. D. A Post-Hartree-Fock Model of Intermolecular Interactions. *J. Chem. Phys.* **2005**, *123*, 024101. (d) Becke, A. D. Density-Functional Exchange-Energy Approximation with Correct Asymptotic Behavior. *Phys. Rev. A* **1988**, *38*, 3098−3100. (e) Lee, C.; Yang, W.; Parr, R. G. Development of the Colle-Salvetti Correlation-Energy Formula into a Functional of the Electron Density. *Phys. Rev. B* **1988**, *37*, 785−789.

(15) (a) Van Lenthe, E.; Baerends, E. J. Optimized Slater-Type Basis Sets for the Elements 1-118. *J. Comput. Chem.* **2003**, *24*, 1142−1156. (b) Fonseca Guerra, C.; Bickelhaupt, F. M.; Snijders, J. G.; Baerends, E. J. Hydrogen Bonding in DNA Base Pairs: Reconciliation of Theory and Experiment. *J. Am. Chem. Soc.* **2000**, *122*, 4117−4128.

https://doi.org/10.1021/acsearthspacechem.1c00433
ACS Earth Space Chem. 2022, 6, 766−774

(16) (a) Van Lenthe, E.; Baerends, E. J.; Snijders, J. G. Relativistic Regular Two-Component Hamiltonians. *J. Chem. Phys.* **1993**, *99*, 4597−4610. (b) Van Lenthe, E.; Ehlers, A.; Baerends, E.-J. Geometry optimizations in the zero order regular approximation for relativistic effects. *J. Chem. Phys.* **1999**, *110*, 8943−8953.
(17) Van Lenthe, E.; Baerends, E. J.; Snijders, J. G. Relativistic Total Energy Using Regular Approximations. *J. Chem. Phys.* **1994**, *101*, 9783−9792.
(18) Franchini, M.; Philipsen, P. H. T.; Visscher, L. The Becke Fuzzy Cells Integration Scheme in the Amsterdam Density Functional Program Suite. *J. Comput. Chem.* **2013**, *34*, 1819−1827.
(19) Bickelhaupt, F. M.; Baerends, E. J. Kohn-Sham Density Functional Theory: Predicting and Understanding Chemistry. In *Reviews in Computational Chemistry*; Wiley, 2000; Vol. *15*.
(20) Bickelhaupt, F. M.; Solà, M.; Fonseca Guerra, C. Structure and Bonding of Methyl Alkali Metal Molecules. *J. Mol. Model.* **2006**, *12*, 563−568.
(21) Van Gisbergen, S. J. A.; Snijders, J. G.; Baerends, E. J. Implementation of Time-Dependent Density Functional Response Equations. *Comput. Phys. Commun.* **1999**, *118*, 119−138.
(22) (a) Yanai, T.; Tew, D. P.; Handy, N. C. A New Hybrid Exchange-Correlation Functional Using the Coulomb-Attenuating Method (CAM-B3LYP). *Chem. Phys. Lett.* **2004**, *393*, 51−57. (b) Seth, M.; Ziegler, T. Range-Separated Exchange Functionals with Slater-Type Functions. *J. Chem. Theory Comput.* **2012**, *8*, 901−907.
(23) (a) Narsaria, A. K.; Ruijter, J. D.; Hamlin, T. A.; Ehlers, A. W.; Fonseca Guerra, C.; Lammertsma, K.; Bickelhaupt, F. M. Performance of TDDFT Vertical Excitation Energies of Core-Substituted Naphthalne Diimides. *J. Comput. Chem.* **2020**, *41*, 1448−1455. (b) Besalú-Sala, P.; Voityuk, A. A.; Luis, J. M.; Solà, M. Evaluation of charge-transfer rates in fullerene-based donor−acceptor dyads with different density functional approximations. *Phys. Chem. Chem. Phys.* **2021**, *23*, 5376−5384.
(24) Albright, T. A.; Burdett, J. K.; Whangbo, W. H. *Orbital Interactions in Chemistry*; John Wiley & Sons: Hoboken, 2013.

https://doi.org/10.1021/acsearthspacechem.1c00433
ACS Earth Space Chem. 2022, 6, 766−774